THE JOURNAL OF BIOLOGICAL CHEMISTRY VOL. 287, NO. 22, pp. 18067–18077, May 25, 2012

C-terminal Acidic Cluster Is Involved in Ca^{2+}-induced Regulation of Human Transient Receptor Potential Ankyrin 1 Channel*[S]

Received for publication, January 12, 2012, and in revised form, March 20, 2012 Published, JBC Papers in Press, March 29, 2012, DOI 10.1074/jbc.M112.341859

Lucie Sura[‡], Vlastimil Zíma[§], Lenka Marsakova[‡], Anna Hynkova[‡], Ivan Barvík[§], and Viktorie Vlachova[‡1]

From the [‡]Department of Cellular Neurophysiology, Institute of Physiology, Academy of Sciences of the Czech Republic, Videnska 1083, 142 20 Prague 4, Czech Republic and the [§]Division of Biomolecular Physics, Institute of Physics, Faculty of Mathematics and Physics, Charles University, Ke Karlovu 5, 121 16 Prague 2, Czech Republic

Background: TRPA1 channel is modulated by Ca^{2+}, but the molecular mechanisms are unclear.
Results: Mutations in the distal C-terminal acidic domain altered Ca^{2+} dependence of TRPA1.
Conclusion: The C-terminal acidic cluster is involved in the Ca^{2+}-induced potentiation and inactivation of TRPA1.
Significance: Identification of the Ca^{2+}-dependent domain is important for understanding the role of TRPA1 in chemical nociception.

The transient receptor potential ankyrin 1 (TRPA1) channel is a Ca^{2+}-permeable cation channel whose activation results from a complex synergy between distinct activation sites, one of which is especially important for determining its sensitivity to chemical, voltage and cold stimuli. From the cytoplasmic side, TRPA1 is critically regulated by Ca^{2+} ions, and this mechanism represents a self-modulating feedback loop that first augments and then inhibits the initial activation. We investigated the contribution of the cluster of acidic residues in the distal C terminus of TRPA1 in these processes using mutagenesis, whole cell electrophysiology, and molecular dynamics simulations and found that the neutralization of four conserved residues, namely Glu^{1077} and Asp^{1080}–Asp^{1082} in human TRPA1, had strong effects on the Ca^{2+}- and voltage-dependent potentiation and/or inactivation of agonist-induced responses. The surprising finding was that truncation of the C terminus by only 20 residues selectively slowed down the Ca^{2+}-dependent inactivation 2.9-fold without affecting other functional parameters. Our findings identify the conserved acidic motif in the C terminus that is actively involved in TRPA1 regulation by Ca^{2+}.

The gating of transduction ion channels in response to various potential life-threatening events is a crucial mechanism underlying the function of sensory neurons. Among the channels that act as important signaling molecules involved in the perception of noxious chemical, mechanical, and cold stimuli in primary afferent neurons, there is one specific protein whose unique polymodal activation properties have drawn much attention over recent years for their potential therapeutic applications: the transient receptor potential ankyrin subtype 1 (TRPA1)[2] channel (1, 2). In addition to a host of pungent and other chemicals that either covalently interact with (isothiocyanates, cinnamaldehyde, acrolein, and allicin) or bind to TRPA1 (cannabinoids, icilin, eugenol, thymol, and nicotine), the channel can also be activated by deep cooling (<17 °C) or depolarizing (>+100 mV) voltages (3–10).

One of the ubiquitous and probably the most important physiological activators of TRPA1 are calcium ions (Ca^{2+}), which enter through the channel or are released from internal stores and, depending on the activation state of the channel, dynamically control its critical properties such as unitary conductance, ion selectivity, channel opening probability (8, 11–13), and surface expression levels (14). At micromolar concentrations, Ca^{2+} ions activate the channel from the intracellular side ($EC_{50} = 0.9 - 6\ \mu M$) (15, 16) and strongly potentiate its chemically and voltage-induced responses. This potentiation is followed by an almost complete and irreversible inactivation, and both processes are accelerated at higher intracellular concentrations of Ca^{2+} (17). Although physiologically extremely important, the molecular mechanisms of Ca^{2+}-dependent activation and inactivation are still a matter of controversy.

The obvious candidates for a domain through which Ca^{2+} could modulate TRPA1 are acidic residues on the intracellular side of TRPA1; unfortunately, information about the potential role of this portion of the receptor is still very scarce, and it is difficult to single out, in the human isoform, from the 112 cytoplasmic acidic residues. As for the cytoplasmic C terminus, evidence for the important functional roles of charged regions came from recent studies identifying a number of basic residues that confer both chemical and voltage sensitivity to the TRPA1 channel, several of them located within or near the two penultimate α-helices H4 and H5 (18). These two predicted helices flank a loop containing a highly conserved acidic stretch of amino acids, ^{1077}ETEDDD^{1082} (see Fig. 1*A*), and sharing sub-

* This work was supported by Czech Science Foundation Grant 305/09/0081, Research Project Fund of the Academy of Sciences of the Czech Republic Grant AV0Z50110509, and Ministry of Education, Youth and Sports of the Czech Republic Grants 1M0517, MSM0021620835, SVV-2010-261 304, and GAUK 426311.
[S] This article contains supplemental Fig. S1.
[1] To whom correspondence should be addressed: Inst. of Physiology AS CR, Videnska 1083, 142 20 Prague 4, Czech Republic. Tel.: 420-29644-2711; Fax: 420-29644-2488; E-mail: vlachova@biomed.cas.cz.

[2] The abbreviations used are: TRPA1, transient receptor potential ankyrin 1; Cin, cinnamaldehyde; RMSD, root mean square deviation.

stantial sequence similarity with the Ca^{2+}-binding domain found in the hBest1 channel (19) or the so-called Ca^{2+} bowl domain of the superfamily of BK channels (20). Here we examined the role of the above conserved acidic sequence motif and found that it is involved in the Ca^{2+}-mediated modulation of TRPA1.

MATERIALS AND METHODS

Expression and Constructs of hTRPA1 Channel—HEK293T cells were cultured in Opti-MEM I medium (Invitrogen) supplemented with 5% FBS as described previously (21, 22). The cells were transiently co-transfected with 300–400 ng of cDNA plasmid encoding wild-type or mutant human TRPA1 (wild type in the pCMV6-XL4 vector, OriGene) and with 300 ng of GFP plasmid (TaKaRa) per 1.6-mm dish using the magnet-assisted transfection (IBA GmbH) method. The cells were used 24–48 h after transfection. At least two independent transfections were used for each experimental group. The wild-type channel was regularly tested in the same batch as the mutants. For membrane-targeting experiments, we used the C-terminally GFP-tagged mutant D1080A of hTRPA1 (wild type in the pCMV6-AC-GFP vector; OriGene) and the cyan fluorescent protein-tagged pleckstrin homology domain of phospholipase C δ1 (kindly provided by Tamas Balla, NICHD, National Institutes of Health, Bethesda, MD). For fluorescence measurements, we used the Cell^R imaging system based on an Olympus IX-81 inverted microscope (Olympus) equipped with a dual emission setup (Dual-View Optical Insights), a Polychrome V polychromator (Till Photonics), and a Hamamatsu Orca ER camera (Hamamatsu Photonics). Intensity profiles were measured using the program ImageJ (National Institutes of Health). The mutants were generated by PCR using the QuikChange XL site-directed mutagenesis kit (Stratagene) and confirmed by DNA sequencing (ABI PRISM 3100; Applied Biosystems).

Electrophysiology—Whole cell membrane currents were recorded by employing an Axopatch 200B amplifier and pCLAMP 10 software (Molecular Devices). Patch electrodes were pulled from a glass tube with a 1.65-mm outer diameter. The tip of the pipette was heat-polished, and its resistance was 3–5 MΩ. Series resistance was compensated by at least 70% in all recordings. The experiments were performed at room temperature (23–25 °C). Only one recording was performed on any one coverslip of cells to ensure that recordings were made from cells not previously exposed to chemical stimuli. Conductance-voltage (*G-V*) relationships were obtained from steady-state whole cell currents measured at the end of voltage steps from −80 to +200 mV in increments of +20 mV. Voltage-dependent gating parameters were estimated by fitting the conductance $G = I/(V - V_{rev})$ as a function of the test potential V to the Boltzmann equation: $G = [(G_{max} - G_{min})/(1 + \exp(-zF(V - V_{½})/RT))] + G_{min}$, where z is the apparent number of gating charges, $V_{½}$ is the half-activation voltage, G_{min} and G_{max} are the minimum and maximum whole cell conductance, V_{rev} is the reversal potential, and F, R, and T have their usual thermodynamic meaning. A system for rapid superfusion of the cultured cells was used for drug application (23). The extracellular bath solutions contained: 150 mM NaCl and 10 mM HEPES, with an added 2 mM HEDTA for the Ca^{2+}-free solution, and 2 or 10 mM $CaCl_2$, for the Ca^{2+}-containing solutions, adjusted to pH 7.3 with NaOH, 300 mOsm. The *I-V* relationships were measured in the bath solution containing 160 mM NaCl, 2.5 mM KCl, 1 mM $CaCl_2$, 2 mM $MgCl_2$, 10 mM HEPES, 10 mM glucose, adjusted to pH 7.3 and 320 mOsm. The whole cell pipette solution contained the high buffer internal solution: 145 mM CsCl, 5 mM EGTA, 3 mM $CaCl_2$, 10 mM HEPES, 2 mM MgATP, pH 7.3, adjusted with CsOH, 320 mOsm. The pipette solution containing 100 μM free Ca^{2+} was obtained by adding 10.24 mM Ca^{2+} and 10 mM EGTA to the internal solution. Cinnamaldehyde solution was prepared prior to use from a 0.1 M stock solution in Me_2SO. All of the chemicals were purchased from Sigma-Aldrich.

Homology Modeling and Molecular Dynamics Simulations—The structure of the human BK channel was obtained from the Protein Data Bank (code 3MT5). The BK-TRPA1 chimera was constructed by replacing Ca^{2+} bowl residues (20) with homologous residues from human TRPA1. Sequences were aligned with ClustalW software (24) and then manually refined to ensure the alignment of conserved residues in the TRPA1 channel matches calcium-binding residues in the Ca^{2+} bowl of the BK channel. A model of the chimera was built using the software package MODELLER (25) resulting in 10 candidate models. The best structure was selected according to the MODELLER objective function, deviation of unmodified parts of the channel from the template and visual inspection. An all-atom structure was generated using the program LEaP from the AMBER suite (26) using the Amber99SB force field and TIP3P water model. One calcium ion and sulfate ion was added at a location corresponding to the template. Total net charge of the structure was neutralized using 17 sodium ions, and the structure was solvated with 21,109 water molecules. The initial equilibration of the system was performed using NAMD2.7 (27) with a time step of 1 fs, cutoff 10 Å, Particle Mesh Ewald grid size of 128 × 128 × 128, Langevin damping 5/ps. The system was first minimized for 10,000 steps and then thermalized to 310 K and equilibrated at 1 atm for 1 ns. Volume and potential energy was monitored and reached stable values. For production runs, we used the ACEMD software package (28) running on a local work station equipped with an Nvidia GPU. The simulations were run in the NVT ensemble with the same parameters as for equilibration, except a time step of 4 fs enabled by the hydrogen mass repartition scheme (29). Data were analyzed using the program PTRAJ from the AMBER suite (26) and visualized using VMD (30).

Statistical Analysis—All of the data were analyzed using pCLAMP 10 (Molecular Devices), and curve fitting and statistical analyses were done in SigmaPlot 10 (Systat Software). Statistical significance was determined by Student's *t* test or the analysis of variance; differences were considered significant at $p < 0.05$, where not stated otherwise. For statistical analysis of T_{50} data, a logarithmic transformation was used to achieve normal distribution. All of the data are presented as the means ± S.E.

RESULTS

Truncations in C Terminus Reveal Region Involved in Ca^{2+}-dependent Inactivation—We set out to investigate the Ca^{2+}-dependent potentiation and Ca^{2+}-dependent inactivation in human TRPA1 channels transiently expressed in HEK293T

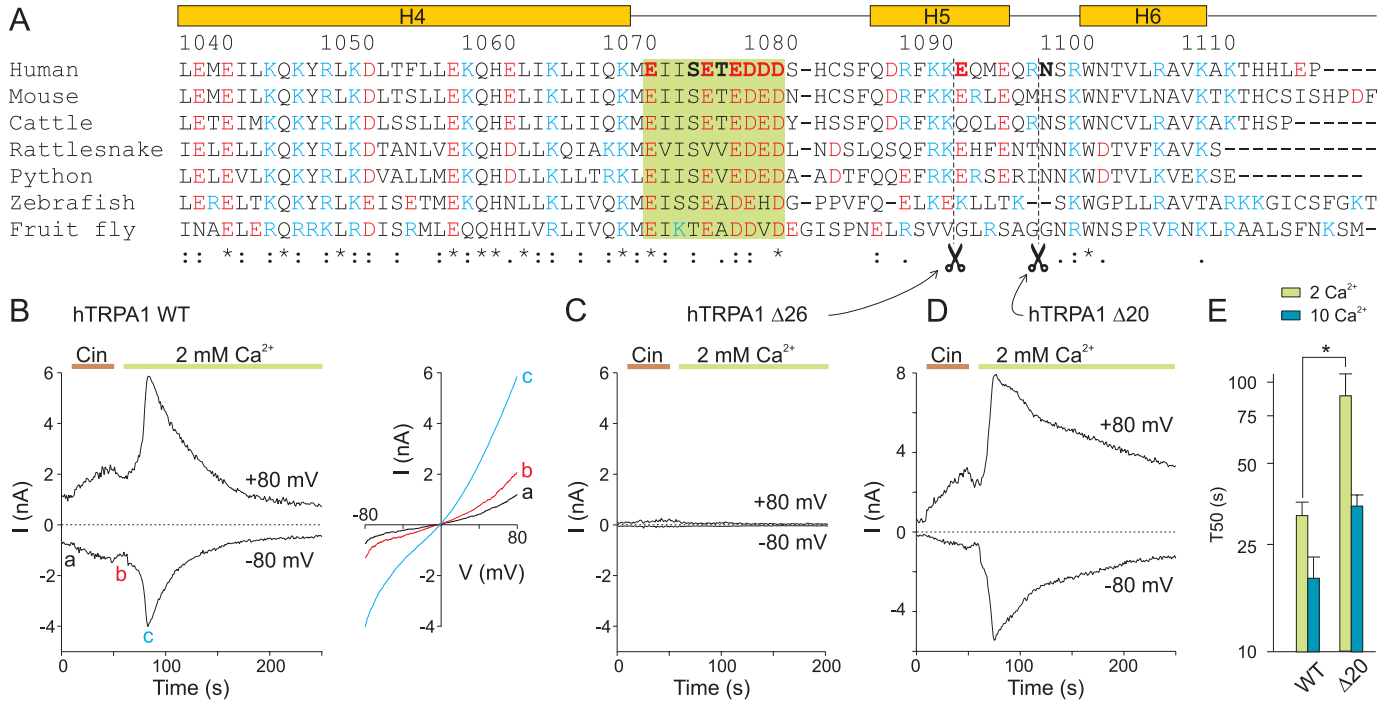

FIGURE 1. **Truncations in C terminus reveal region involved in Ca^{2+}-dependent inactivation.** *A*, alignment of distal C terminus of TRPA1 from various species. The predicted secondary structure for hTRPA1 is indicated above the alignment. The region of interest is *boxed*. The residues in human TRPA1 that were mutated in this study are indicated in *bold type*. *B*, time course of representative whole cell currents through human TRPA1 measured at +80 mV and −80 mV as marked. The application of 100 μM Cin and subsequent addition of 2 mM Ca^{2+} are indicated above. The *right panel* shows current-voltage relationships of traces measured at times indicated by *a*, *b*, and *c*. *C* and *D*, voltage-ramp protocol as in *B* used for truncation mutants. Note the obviously slower inactivation of the TRPA1-Δ20 truncation mutant upon the addition of 2 mM Ca^{2+} to the bath solution compared with WT in *B*. *E*, average rate of current decay represented as T_{50} for wild-type TRPA1 and truncation mutant TRPA1-Δ20. To obtain a similar rate of inactivation to the wild-type TRPA1, a 5-fold higher concentration of calcium needed to be introduced for the TRPA1-Δ20 mutant. *, $p = 0.006$, Student's *t* test. The data represent the means ± S.E.; $n \geq 6$ for wild type and $n \geq 3$ for mutant.

cells. Because some activation properties considerably differ between the mammalian TRPA1 orthologs, we first quantified the effects of Ca^{2+} by exploiting the same stimulation protocol as has been previously used by Wang *et al.* (17) for a detailed characterization of the rat TRPA1 variant (Fig. 1*B*). The membrane potential was ramped from −80 to +80 mV (1 V/s), and whole cell membrane currents were measured in the absence of extracellular Ca^{2+} and in the presence of agonist (cinnamaldehyde, Cin, 100 μM for 40 s). The agonist was then washed out for 10 s, and Ca^{2+} at a concentration of 2 mM or 10 mM was added to the extracellular solution. Intracellular Ca^{2+} was buffered with 5 mM EGTA in the patch pipette. In accordance with (17), Cin evoked slowly developing currents (2.4 ± 0.2 nA at +80 mV after 40 s, $n = 38$) that slightly relaxed (by 17 ± 1%) to a lower maintained level upon washout. The addition of Ca^{2+} to the bath solution induced a marked potentiation that was followed by an inactivation that was almost complete within 1 min (Fig. 1*B*). The degree of Ca^{2+}-induced potentiation was quantified as the fold increase in the amplitude after the addition of Ca^{2+} with respect to the preceding current level. For 2 mM Ca^{2+}, this value was 4.0 ± 0.4 at +80 mV and 6.0 ± 1.1 at −80 mV ($n = 24$), which is higher than that for the rat ortholog and is in good agreement with the value previously reported for human TRPA1 (17). The 10–90% rise time for potentiation was clearly dependent on external Ca^{2+}, being 7.8 ± 1.0 and 2.5 ± 0.5 s ($n = 22$ and 16) for 2 and 10 mM Ca^{2+}, respectively.

For Ca^{2+}-dependent inactivation, the decay was adequately described using a half-decay time, relative to the peak (T_{50}). After the introduction of 2 mM Ca^{2+}, the currents decayed to 50% of their peak value in 31.9 ± 4.0 s at +80 mV and in 18.9 ± 2.0 s at −80 mV ($n = 19$). At 10 mM Ca^{2+}, the inactivation was substantially faster (16.3 ± 3.0 s at +80 mV and 11.2 ± 2.0 s at −80 mV; $n = 15$), which was most likely the cause of a concomitant reduction in the degree of Ca^{2+}-induced potentiation (3.1 ± 0.4), compared with 2 mM Ca^{2+} ($p = 0.15$). We did not find any clear correlation between T_{50} and the degree of Ca^{2+}-dependent potentiation ($r = -0.35$, 2 mM Ca^{2+}, +80 mV; $n = 19$; Spearman's rank order correlation), which supports the previous suggestion that the inactivation of TRPA1 is not strictly coupled to potentiation (11, 17, 31).

Having established the main characteristics of the Ca^{2+}-dependent modulation for wild-type channels, we constructed a series of mutants in which the negative charges in the C-terminal subregion Glu^{1073}–Asp^{1082} were individually neutralized by alanine substitution. In addition, two charge-reversing mutations were created for the acidic cluster glutamates, E1077K and E1079K. Furthermore, to test the overall structural requirements of the distal C terminus for channel activation, we introduced stop codons at Glu^{1094} and Asn^{1100}, resulting in two C-terminal truncation mutants, TRPA1-Δ20 and TRPA1-Δ26. The conservation of the primary structure of this region and the residues chosen for mutagenesis are summarized and depicted in Fig. 1*A*.

Mutation TRPA1-Δ26 did not produce measurable currents in response to any of the stimuli tested, thus preventing further evaluation (Fig. 1*C*). In contrast, functional channels were

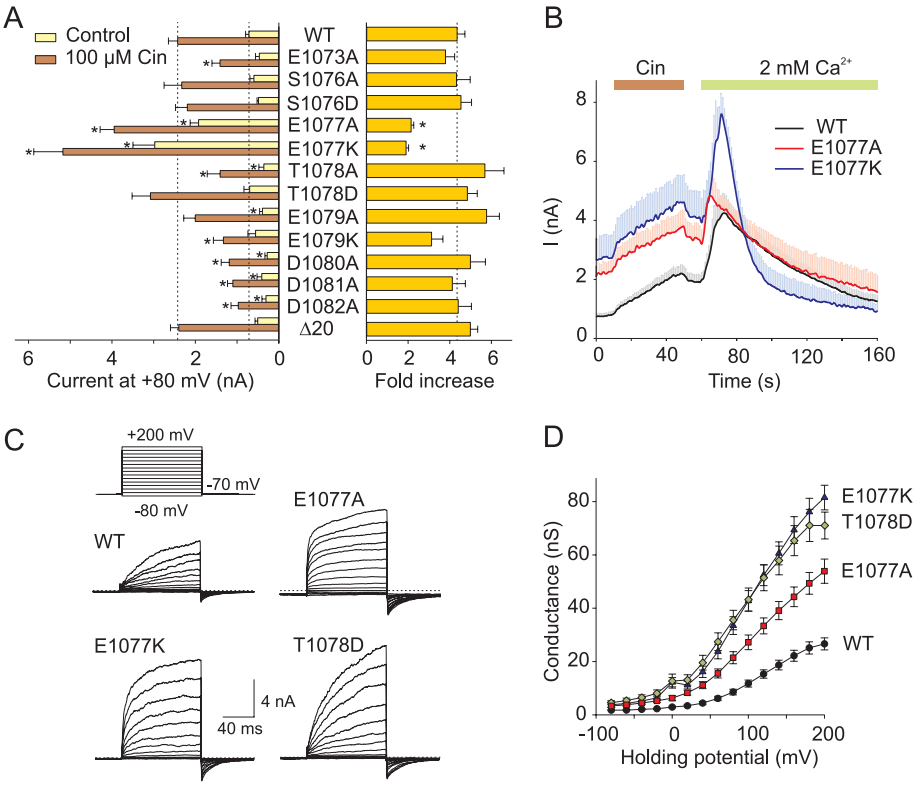

FIGURE 2. **Mutations in C-terminal acidic region alter voltage and cinnamaldehyde sensitivity of TRPA1.** *A*, *left bar graph* depicts average TRPA1 currents at +80 mV in Ca^{2+}-free extracellular solution before (control) and after 40 s of 100 μM Cin exposure. The *right bar graph* indicates relative activation by Cin for wild-type channel and individual mutants. The data represent the means ± S.E.; $n \geq 6$. The *asterisks* indicate significant differences between mutant and wild-type TRPA1. *, $p < 0.05$, unpaired *t* test. *Broken vertical lines* indicate the mean values obtained from wild-type TRPA1. *B*, average currents at +80 mV for wild-type TRPA1 and gain of function mutants E1077A and E1077K. The *horizontal bars* above the records indicate the duration of Cin and Ca^{2+} application. Note the difference in basal activation level at the very beginning of the record. The data represent the means ± S.E. for $n \geq 6$. *C*, representative current traces in response to indicated voltage step protocol (holding potential, −70 mV; voltage steps from −80 to +200 mV; increment +20 mV), recorded ~1 min after whole cell formation. The bath solution contained 160 mM NaCl, 2.5 mM KCl, 1 mM $CaCl_2$, 2 mM $MgCl_2$, 10 mM HEPES, 10 mM glucose. *D*, average conductances obtained from voltage step protocols as in *C*. The data represent the means ± S.E.; $n \geq 8$.

obtained with the TRPA1-Δ20 truncation mutant (Fig. 1*D*). Compared with wild-type TRPA1, this mutant exhibited strikingly slower inactivation upon the addition of Ca^{2+} (T_{50} of 89.0 ± 18.4 s for 2 mM Ca^{2+} and 34.7 ± 6.0 s for 10 mM Ca^{2+}; $p < 0.01$; $n = 6$ and 3; Fig. 1*E*). In other respects, this truncation mutant exhibited a normal degree of Ca^{2+}-induced potentiation (3.0 ± 0.1; $p = 0.63$; $n = 6$) and a normal responsiveness to voltage and Cin (Fig. 2*A*). The finding that truncation of the C terminus by a further six residues was deleterious indicates an important functional role for the distal part of the C terminus, particularly a likely structural role of the predicted α-helix H5. These initial screenings identified the distal C terminus as a critical modulatory domain of TRPA1 involved in its Ca^{2+}-dependent inactivation, and we therefore further examined whether the acidic region preceding this H5 helix could play its presumed role of a high affinity Ca^{2+} sensing site.

Mutations in C Terminus Reveal Strongly Sensitizing TRPA1 Phenotypes—The functionality of all constructed mutants was compared by measuring the maximum outward currents at +80 mV, in the absence and presence of 100 μM Cin. We detected a dramatic increase in the amplitude of the outward currents induced by voltage ramps in control Ca^{2+}-free bath solution through the E1077A and E1077K mutant channels at the 0.01 probability level (Fig. 2, *A* and *B*). Also, the conductance to voltage (*G-V*) relationships for these two mutants were significantly shifted toward less depolarizing potentials (the voltage for half-maximal activation, V_{50}, 110.8 ± 5.8 and 104.5 ± 6.0 mV; $n = 18$ and 12), compared with wild-type TRPA1 channels (128.0 ± 2.7 mV; $n = 57$; Fig. 2, *C* and *D*). In E1077K, but not in E1077A, the inactivation produced by the introduction of 2 mM Ca^{2+} was significantly faster compared with the wild type ($T_{50} = 14.4 \pm 5.5$ s; $n = 6$; $p < 0.05$), and the currents decayed to a steady value 66 ± 10% below their initial basal activity levels (Fig. 2*B*). In both mutants, E1077A and E1077K, the degree of potentiation of Cin responses by 2 mM Ca^{2+} was markedly reduced (2.5 ± 0.4; $n = 6$; $p = 0.087$ and 1.9 ± 0.3; $n = 7$; $p = 0.009$), obviously because of their initial close to saturation state at +80 mV.

We suspected that this sensitizing effect reflected either a gain of function (constitutively active) phenotype or tonic activation caused by an increased expression of the functional mutant channels on the cell surface. Indeed, within our region of interest, a sequence prediction analysis revealed two strong consensus phosphorylation motifs containing serine 1076 and threonine 1078, both predicted to be targeted by casein kinase CK2 (as determined from the prediction servers NetPhosK or NetPhorest). A similar phosphorylatable acidic cluster has been reported to constitute a cytosolic sorting motif that controls the trafficking and surface expression of some ion channels, including TRPA1-related TRPP2 and TRPV4 (32). To test this possi-

bility, we constructed additional four mutants in which either serine or threonine were replaced by either alanine or aspartate to mimic the nonphosphorylated and phosphorylated forms of the protein, respectively. To our surprise, mutation T1078D resulted in TRPA1 channels whose conductance to voltage (*G-V*) relationships were also strongly augmented (from 27 ± 2 to 71 ± 5 nS at +200 mV; $n = 59$ and $n = 8$) and shifted toward less depolarizing potentials (V_{50}, 98.1 ± 6.8 mV; Fig. 2*D*). This mutant responded relatively normally to Cin in Ca^{2+}-free bath solution (Fig. 2*A*) but had a faster 10–90% rise time of outward current potentiation of Cin responses upon the addition of 2 mM Ca^{2+} (2.7 ± 0.2 s; $n = 4$; $p < 0.05$) and slightly ($p = 0.094$) faster inactivation (16.1 ± 5.2 s; $n = 5$) compared with the T_{50} for wild-type channels.

Whereas T1078D was observed to have large effects on voltage-dependent activation when using the voltage-step protocol (Fig. 2, *C* and *D*), only modest effects on voltage- and cinnamaldehyde-dependent activation were seen when the standard voltage-ramp protocol was utilized (Fig. 2*A*). This apparent divergence seemed to be due to the alterations in the onset kinetics upon voltage changes ($\tau_{on} = 36 \pm 3$ ms *versus* 59 ± 5 ms for wild-type; measured at +160 mV; $n = 6$ and 17; Fig. 2*C*) and indicates that mutation T1078D affected the gating kinetics of TRPA1. This interpretation is further supported by our finding that mutation T1078A exhibited substantially reduced responses to voltage and Cin and was capable of strong potentiation by 2 mM Ca^{2+} (5.5 ± 0.8; $n = 6$; $p = 0.125$). The nonphosphorylatable mutant S1076A and the phosphorylation-mimicking S1076D mutant channels were otherwise normal in all general aspects of functionality.

This series of experiments indicates that a single mutation at Glu^{1077}, or the introduction of an additional negative residue at Thr^{1078} are both likely to destabilize the charge balance at the highly acidic C-terminal cluster of TRPA1. The findings that a neutralizing or charge-reversing mutation at Glu^{1077} had sensitizing effects support the notion that the functional changes caused by mutations are likely to be steric or local, rather than affected by increased membrane insertion of the channels because of disruption of a phosphorylation consensus. Moreover, single point mutations at the specific residues, located in the primary sequence far from the membrane proximal regions, are capable of increasing the sensitivity of TRPA1 to membrane voltage without affecting its responsiveness to Cin. In other words, a pathway distinct from voltage-dependent modulation and covalent modification effectively controls the activity of TRPA1 via conformational changes in the C-terminal acidic region.

Asp^{1080}, Asp^{1081}, and Asp^{1082} Are Residues Most Involved in Ca^{2+}-induced Potentiation of TRPA1—When the maximum Cin-induced outward currents were related to the control voltage-induced responses obtained at the same membrane potential of +80 mV, none of the single mutations, apart from E1077A and E1077K, exhibited a substantially decreased relative sensitivity to Cin compared with wild-type TRPA1, as depicted in Fig. 2*A*. What we found, however, was that the kinetics of the Ca^{2+}-dependent potentiation were dramatically changed in four out of the six charge-neutralized mutants: E1073A, D1080A, D1081A and D1082A. The former mutation strongly increased the degree of Ca^{2+}-dependent potentiation at both Ca^{2+} concentrations and caused a delay in the peak potentiation time in a significant number of cells (Fig. 3, *A* and *B*). Distinct phenotypes were generated by the latter three neutralizing mutations. Not only did these mutations lead to a marked slowing down of the rise time and delayed the peak potentiation time, they also led to a strongly reduced averaged degree of potentiation observed within an interval of ~120 s after the introduction of Ca^{2+}, which was readily apparent from the averaged current traces obtained from all cells tested (Fig. 3*A*). Ca^{2+}-dependent potentiation was most apparently blunted in the D1080A mutant. In five of ten D1080A-expressing cells that were treated with 2 mM Ca^{2+} and in three out of seven cells treated with 10 mM Ca^{2+}, no potentiation at all was observed within the time interval tested (3–4 min); instead, the Cin-induced currents decayed in the presence of Ca^{2+} to their initial value obtained before the agonist was applied to these cells (Fig. 3*A*). Weaker but similar effects were observed in D1081A and D1082A. The former mutation produced currents that also exhibited a "delayed phenotype", but when measured over a period longer than the median time to peak for the wild type (14 s), they frequently attained a similar degree of potentiation to wild-type TRPA1 (Fig. 3, *A* and *B*).

For wild-type channels, the peak potentiation time, measured from the time at which 2 mM Ca^{2+} was introduced, varied from 4 s to more than 30 s with a median of 14 s ($n = 22$) and this value became lower and normally distributed around the mean of 6.0 ± 1.1 s when the external Ca^{2+} concentration was increased to 10 mM ($n = 16$; Fig. 3*C*). The maximum potentiation time has been previously shown to depend on external Ca^{2+} concentration (17), and thus the observed changes in the kinetics of the Ca^{2+}-dependent modulation in the mutants shown in Fig. 3*A* could be due to a decreased sensitivity to external Ca^{2+}. Because the data for peak potentiation time in wild-type TRPA1 was not normally distributed, to achieve reliable statistical significance in the distribution for the mutants would require an unrealistically large number of cells to be tested for each group. However, it was still evident that the period of maximum potentiating effect was delayed in a considerable proportion of cells expressing D1080A, D1081A and D1082A (Fig. 3*A* and supplemental Fig. S1). The most affected mutant, D1080A, was functionally well expressed (Fig. 2*A*) and appeared to be correctly targeted to the cell membrane (Fig. 3*D*). In this mutant, the addition of a higher concentration of external Ca^{2+} (10 mM) reduced the 10–90% rise time (from 18.7 ± 7.2 s to 7.0 ± 2.4 s; measured from five and four responding cells; Fig. 4*A*), accelerated inactivation (Fig. 4*B*), and increased both the degree and probability of occurrence of the maximum Ca^{2+}-induced potentiating effect (Fig. 4*C*).

The high buffer internal solution used in our experiments was estimated to contain 150 nM free Ca^{2+}, which approximately corresponds to the basal intracellular concentration of Ca^{2+}. We therefore further tested whether allowing the internal concentration of Ca^{2+} to increase would change the activity, especially for the D1080A mutant, which exhibited the most significantly modified kinetics of Ca^{2+}-dependent potentiation. We compared the degree of potentiation and the rate of inactivation in cells dialyzed with an intracellular solution containing 100 μM free Ca^{2+} (Fig. 4, *C* and *D*). Under these condi-

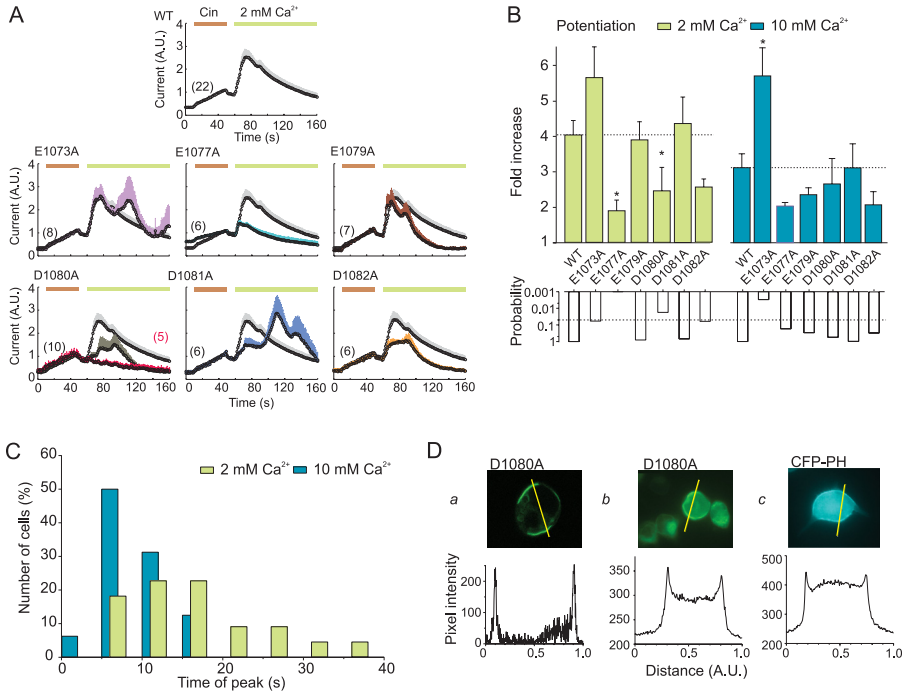

FIGURE 3. **Potentiation of TRPA1 mutants by extracellular Ca^{2+}.** *A*, average TRPA1 currents evoked in response to 40 s of exposure to 100 μM Cin and subsequent addition of 2 mM Ca^{2+} as indicated by *horizontal bars*. The average current for the wild type is shown for comparison in *gray* in each plot. The currents are normalized to their maximal cinnamaldehyde responses obtained prior to the addition of Ca^{2+} to the bath solution. The data represent the means ± S.E. for the number of cells indicated. For D1080A, the average current for nonpotentiated cells (in *red*) is overlaid onto the average current from all cells. *B*, average data from experiments as in *A*. Calcium-induced potentiation was measured as the fold increase in current, measured at +80 mV, following the addition of 2 mM (*left bar graph*) or 10 mM (*right bar graph*) extracellular Ca^{2+}. The *asterisks* indicate significant differences between mutant and wild-type TRPA1. *, $p < 0.05$, unpaired *t* test. The *lower bar graph* represents the probabilities obtained from the *t* tests that compared the individual mutants with the wild type. *C*, distribution of time to peak of Ca^{2+}-induced potentiation for wild-type TRPA1 channels. For 2 mM Ca^{2+}, four cells had time-to-peak outside the range of 60 s. *D*, D1080A mutant of hTRPA1 expresses on the surface of HEK293T cells to a similar level as a control molecule containing membrane-targeting motif. *Panel a*, typical confocal image from cell expressing D1080A mutant of the C-terminally GFP-tagged human TRPA1 and a fluorescence intensity profile plotted for the cross-section indicated above. *Panel b*, wide-field fluorescence image of HEK293T cell expressing D1080A mutant of the C-terminally GFP-tagged human TRPA1. The excitation wavelength was 470 nm, and emission was detected at 530 nm. *Below* is a fluorescence intensity profile plotted for the cell and a cross-section (marked by *line*) indicated above. *Panel c*, wide field fluorescence image of a fluorescent marker for the membrane surface, cyan fluorescent protein-tagged pleckstrin homology domain of phospholipase Cδ1 (*CFP-PH*), expressed in another HEK293T cell for comparison. *Below*, typical fluorescence intensity profile plotted for the cell and cross-section indicated above. The excitation wavelength was 430 nm, and emission was detected at 475 nm.

tions, the D1080A mutant channels produced robust currents in response to Cin in Ca^{2+}-free bath solution, and after the addition of external 10 mM Ca^{2+}, the currents were consistently potentiated (2.2 ± 0.4-fold; $n = 5$) without any delay. In contrast, Ca^{2+}-induced responses through wild-type channels dialyzed with the same internal solution were mostly inactivated immediately after the addition of external 10 mM Ca^{2+}, indicating a predominant effect on promoting inactivation over Ca^{2+}-induced potentiation (Fig. 4*C*). Despite differences between D1080A and wild-type channels in the degree of potentiation, we did not detect any difference in the rate of inactivation between D1080A-expressing cells dialyzed with an intracellular solution containing 100 μM free Ca^{2+} (T_{50} of 16.9 ± 4.6 s; $n = 5$) and the wild-type channels ($p = 0.919$) or the D1080A mutant channels (12.1 ± 2.0 s; $p = 0.374$; $n = 4$), measured with the high buffer internal solution. Because the identified mutation D1080A exhibits a normal responsiveness to Cin and approaches the wild-type phenotype when internal Ca^{2+} is allowed to increase to 100 μM, these results suggest that this mutation most likely has an effect on Ca^{2+} affinity.

Molecular Dynamics Simulations Indicate That C-terminal Acidic Cluster Is Capable of Playing Role of High Affinity Ca^{2+}-binding Site—The observations that Asp^{1080} indeed contributes to the Ca^{2+}-dependent modulation of TRPA1, together with the fact that substitutions at Glu^{1077} produced sensitized phenotypes, further supports the idea that the whole region containing the cluster of negative residues is structurally important and involved in the Ca^{2+}-dependent modulation of TRPA1. How could the C-terminal acidic domain in TRPA1 accomplish the role of a high affinity Ca^{2+} sensor?

To address this question, we utilized molecular dynamics simulations to probe the Ca^{2+}-binding capability of the acidic region from TRPA1, using the Ca^{2+} activation apparatus of the human BK channel (20) as the template protein (hSlo1; Protein Data Bank entry code 3MT5). Each of the four α subunits of the high conductance, Ca^{2+}- and voltage-activated potassium BK channel contain two tandem regulatory C-terminal domains (RCK) that form an intracellular gating ring (33). The second of these domains (RCK2) encompasses a primary binding site for Ca^{2+}, known as the Ca^{2+} bowl, which exhibits a considerable sequence similarity to the C-terminal acidic sequence of TRPA1 (Fig. 5*A*). We used homology modeling to replace the stretch of 10 consecutive residues Gln^{889}–Asp^{898} (QFLDQDDDD) in the structure of the Ca^{2+}-binding domain of BK with 10 residues Ile^{1074}–Ser^{1083} (IISETEDDDS) from human TRPA1 (Fig. 5*B*), and using molecular dynamics simulations, we explored whether this region is capable of binding Ca^{2+}. The system was simulated for a total of 200 ns after equilibra-

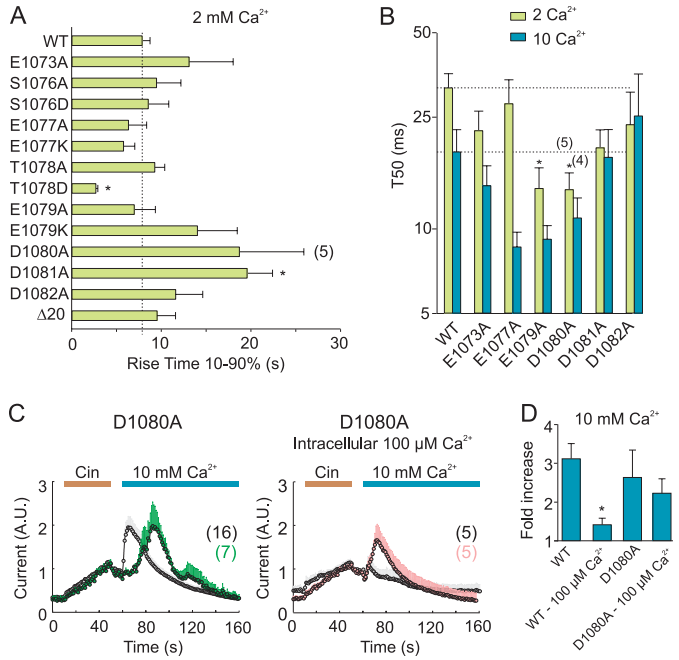

FIGURE 4. **Mutations in C-terminal acidic domain affect kinetics of Ca^{2+}-induced potentiation.** *A*, 10–90% rise time of Ca^{2+}-induced potentiation (2 mM) for wild-type and mutant TRPA1. The *broken vertical line* indicates the mean value obtained from wild-type TRPA1. *B*, average data from experiments as in Fig. 3*A*. Inactivation was measured at +80 mV and quantified as the time, relative to the peak, at which the currents had decayed to 50% of their maximum value. The *broken horizontal lines* indicate the mean values obtained from wild-type TRPA1 for 2 and 10 mM Ca^{2+}. In *A* and *B*, *asterisks* indicate significant differences between mutant and wild-type TRPA1. *, $p < 0.05$, unpaired *t* test. *C*, *left panel*, increasing the concentration of extracellular Ca^{2+} from 2 mM to 10 mM partially restored the Ca^{2+}-induced potentiation in D1080A. *Right panel*, increasing the intracellular Ca^{2+} concentration from 150 nM to 100 μM restored the potentiation of the cinnamaldehyde-induced currents in the D1080A mutant channels. The average current for the wild type is shown for comparison in *gray* in each plot. The currents are normalized to their maximal cinnamaldehyde responses obtained prior to the addition of Ca^{2+} to the bath solution. The data represent the means ± S.E. for the number of cells indicated. *D*, average data from experiments as in *C*, quantified as in Fig. 3*B*. The *asterisk* indicates a significant difference from wild-type TRPA1 measured with the high buffer internal solution containing 5 mM EGTA in the patch pipette. *, $p = 0.01$, unpaired *t* test.

tion. The time course of the root mean square deviation (RMSD) over the 200-ns period indicates that the system was sufficiently relaxed after 70 ns, and the calcium-binding motif was sufficiently relaxed after 110 ns (Fig. 5*C*). The displacement of the calcium ion inside the calcium-binding motif was under 1 Å for most of the simulation (Fig. 5*C*), indicating that the ion was quite stable. A significant increase in RMSD at the end of the simulation was identified to be caused by the loose ends of the polypeptides at residues 833–869. The structure between these residues is missing from the Protein Data Bank structure 3MT5 and is missing from the model structure as well. Therefore, we explored the influence of excluding these loose ends (residues 830–862) from the RMSD calculation (Fig. 5*C*). Because these residues do not interact with the residues of interest, except for weak interactions in the last 25 ns of the run, we do not expect this to have significant influence on the simulation results presented here.

The results of this computational experiment confirm that the calcium ion is bound in the structure and thus prove the ability of the acidic cluster from the TRPA1 C terminus to form a Ca^{2+}-binding domain. Fig. 5*D* depicts the time course of the number of calcium contacts with the protein and in total. The average number of contacts throughout the simulation period was 7.6, which is in good agreement with experimental measurements carried out on various other Ca^{2+}-binding proteins (34). Two residues, Ile^{889} (Ile^{1074} in TRPA1) and Glu^{892} ($Glu1077$), are in contact with the calcium ion via their main chain carbonyl oxygen atoms (Fig. 5*C*). Two residues, Asp^{895} (Asp^{1080}) and Asp^{897} (Asp^{1082}), use oxygen atoms from their side chains for direct contact with the calcium ion. These bonds are largely stable throughout the whole simulation period, which is again in good agreement with the binding mechanism of calcium ions in the Ca^{2+} bowl in the BK cytoplasmic domain (20).

To further test the model and to explore the effects of mutations on the stability of calcium ion binding, we performed additional molecular dynamics simulations using *in silico* alanine mutations: E894A, D895A, D896A, and D897A (E1079A, D1080A, D1081A, and D1082A in TRPA1). Disruptions of the calcium-binding pocket were observed in D895A (D1080A) and in D897A (D1082A) after, respectively, 11 and 4 ns of molecular dynamics simulation (Fig. 6*A*). Mutations E894A (E1079A) and D896A (D1081A) had no effect on the stability of calcium binding during a 20-ns simulation. These findings substantiate the importance of the residues D1080A and D1082A for Ca^{2+} binding.

Next, we examined whether the side chain volume at positions Asp^{1080} and Asp^{1082} is important for the functionality of the channel. Using site-directed mutagenesis, we individually replaced these two residues with isoleucine and measured whole cell responses to Cin in the absence and presence of 2 mM Ca^{2+} (Fig. 6*B*). Similar to what has been observed for D1080A, mutation D1080I produced channels that responded normally to cinnamaldehyde but exhibited strong changes in Ca^{2+}-dependent modulation. In three of seven D1080I-expressing cells that were treated with 2 mM Ca^{2+}, no potentiation at all was observed within the time interval tested (Fig. 6*B*, *left panel*). The D1082I mutant exhibited even more pronounced defects (compared with D1082A and the wild type), yielding channels that produced robust currents in response to Cin in Ca^{2+}-free bath solution, but the addition of external 2 mM Ca^{2+} did not exert any noticeable effect within the time interval tested (Fig. 6*B*, *right panel*). These results indicate that the side chain volume at Asp^{1082} is important for channel function and that isoleucine substitution at this position may create steric hindrance for Ca^{2+} access to the acidic region.

DISCUSSION

In this study, we identify the residues within the distal C-terminal domain of the human ankyrin receptor TRPA1 that when mutated affect the Ca^{2+}- and voltage-dependent gating of the channel. The first key finding of our study is that truncation of the C-terminal domain by 20 amino acids reduces the inactivation of the TRPA1 channel without altering its activation by the thiol-reactive compound cinnamaldehyde or the degree of Ca^{2+}-dependent potentiation. This result provides further support for the previous suggestion that the inactivation mechanism of TRPA1 is not coupled to activation/potentiation (17).

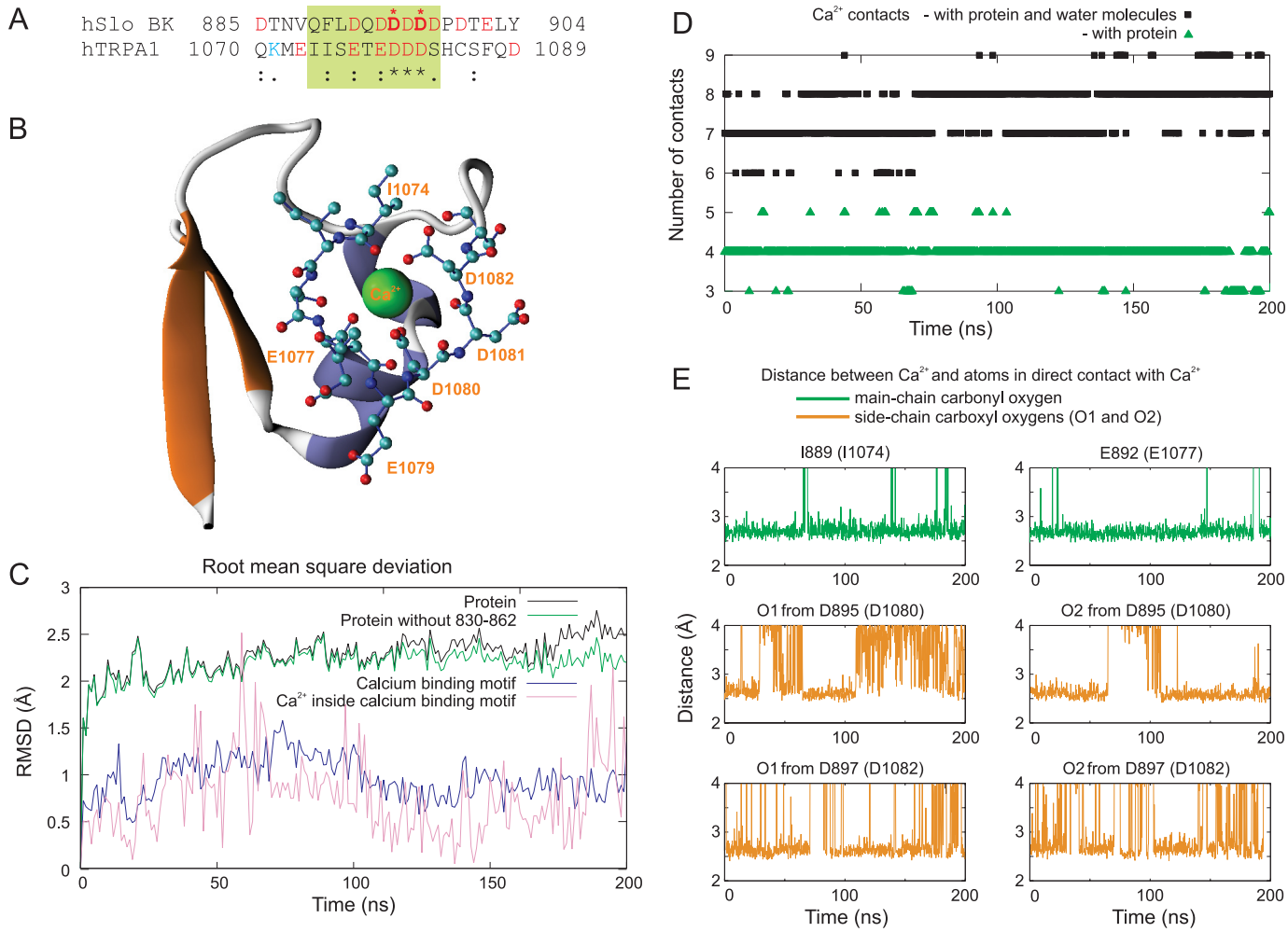

FIGURE 5. **Homology modeling and molecular dynamics simulations of acidic region from TRPA1 based on Ca^{2+} activation apparatus of human BK channel (hSlo1; Protein Data Bank entry code 3MT5) as template protein.** *A*, alignment of Ca^{2+}-binding domain of BK with C-terminal acidic region from human TRPA1. *B*, illustration of calcium-binding site in hSlo1-TRPA1 chimera with surrounding structures. Residues from the TRPA1 protein are shown in ball and stick representation. Snapshot is the frame at 200 ns of the simulation. *C*, RMSD of protein and calcium-binding site. *C* also indicates the displacement of the calcium ion inside of the calcium-binding domain. A significant increase in RMSD at the end of simulation was identified to be caused by loose ends of the polypeptides at residues 833–869, whose structure is not known and was missing from the model structure (see "Materials and Methods"). The system was simulated for a total of 200 ns after equilibration. The time course of RMSD indicated that the system was sufficiently relaxed after 70 ns, and the calcium-binding motif was sufficiently relaxed after 110 ns. The displacement of the calcium ion was less than 1 Å for most of the simulation, indicating that the ion was stable. *D*, number of contacts with Ca^{2+} ion throughout simulation. *E*, lengths of ionic bonds between calcium ion and atoms in calcium-binding site.

Moreover, the inactivation requires Ca^{2+} entry through the activated channel, and thus the structural regions close to the channel pore were proposed to undergo Ca^{2+}-induced conformational changes to regulate TRPA1 gating (11–13). The proximal C-terminal domain of TRPA1 is thought to contain functionally important juxtamembrane helix H1 (Ile^{964}–Lys^{989}) adjacent to the predicted inner vestibule of the channel. We have previously demonstrated that mutations in this domain have strong effects on several aspects of TRPA1 functioning, including changes in its voltage-dependent activation/deactivation kinetics and a significant increase in the current variance at depolarizing potentials (18). We then hypothesized that the pore-forming S6 helix of TRPA1 may extend to the cytoplasmic region so that the proximal helix H1 could directly participate in the regulation of gating or permeation properties of the channel. The new finding that a distal C-terminal structure provides the TRPA1 channel with its ability to respond to external calcium leads to the notion that the quarternary organization of the C-terminal domain includes an intracellular gating ring on the cytoplasmic surface, functionally reminiscent of the Ca^{2+}-dependent operation of the human BK channel gating ring apparatus (20, 35). This hypothesis is further supported by a recent report demonstrating a strong continuous density near the transmembrane region revealed by single-particle electron microscopy (36). Another line of evidence also supports this possibility.

Our second key finding that the two neighboring mutations within the acidic region, E1077K and T1078D, caused a shift in the conductance-voltage (*G/V*) curve to less depolarized membrane voltages indicates that the TRPA1 channel pore might be controlled by voltage via a connection between the distal portion of the C terminus and the putative voltage sensor or the S6-H1 module. Compared with voltage-gated potassium channels, the voltage dependence of TRPA1 is very weak, with the estimated apparent number of gating charges less than 1 (10, 18). It is anticipated that the putative voltage-sensing domain,

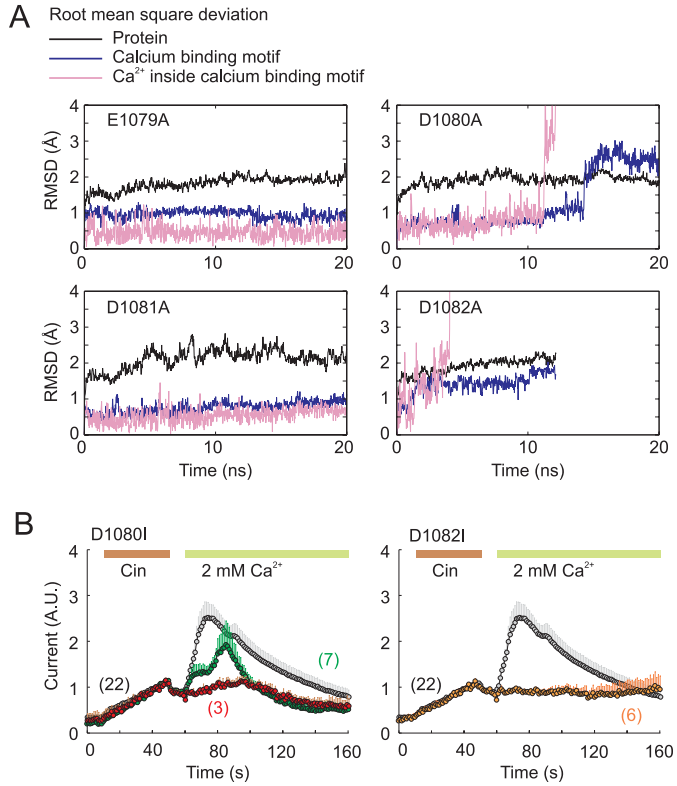

FIGURE 6. **Mutations in C-terminal acidic region.** *A*, molecular dynamics simulations of *in silico* alanine mutations of the BK/TRPA1 chimera. RMSDs of whole protein, calcium-binding site, and displacement of calcium ion in the predicted calcium-binding site for each mutant. Calcium ion was stable in E1079A and D1081A. Disruptions of the calcium-binding pocket were observed in D1080A and in D1082A after 11 and 4 ns of molecular dynamics simulation. The simulation of D1082A (D897A) mutation was particularly unstable, and the calcium ion left the binding site very soon after simulation entered production run. This simulation was interrupted after 10 ns of run. *B*, potentiation of the TRPA1 mutants D1080I and D1082I by extracellular Ca^{2+}. Average whole cell currents evoked in response to 40 s of exposure to 100 μM Cin and subsequent addition of 2 mM Ca^{2+} as is indicated by *horizontal bars*. The average current for the wild type is shown for comparison in *gray* in each plot. The currents are normalized to their maximal cinnamaldehyde responses obtained prior to the addition of Ca^{2+} to the bath solution. The data represent the means ± S.E. for the number of cells indicated. For D1080I, the average current for nonpotentiated cells (in *red*) is overlaid onto the average current from all cells (in *green*).

which has not been identified yet, most likely lies outside the conventionally considered fourth transmembrane segment (S4), because this region does not contain any charged residues at all. Within the S4-S5 linker of human TRPA1, a gain of function point mutation N855S has been identified to exhibit a 5-fold increase in inward currents on activation by cinnamaldehyde, menthol, or the endogenous aldehyde 4-hydroxynonenal at normal resting membrane potentials (37). Removing extracellular Ca^{2+} ions shifts the voltage-dependent activation by approximately +20 mV in both the wild type and the N855S mutant, compatible with the sensitizing effect of Ca^{2+}. This behavior can be explained well by the allosteric model of TRPA1 activation by two different stimuli (38). In addition, the decreased cooperativity of voltage-dependent gating under the Ca^{2+}-free conditions found in N855S indicates that this mutation destabilizes the closed conformation, which could account for a more general effect on channel gating (39) and is consistent with the proposed functional role for the S4-S5 linker in the gating of other thermosensitive TRP channels (40–42).

We do not have a strong structural explanation for the gain of function effects seen in the E1077A, E1077K, and T1078D mutants. The T1078D mutation in particular had large effects on voltage-dependent activation when using the voltage-step protocol, but only modest effects on voltage- and cinnamaldehyde-dependent activation when the standard voltage-ramp protocol was utilized (Fig. 2). We attribute this apparent discrepancy to the fast onset kinetics of the mutant channel upon voltage changes and suggest that Thr^{1078} is implicated in allosteric coupling between the activation site(s) (voltage sensor, Ca^{2+} sensor) and the movement of the gate. As for the proposed role of the whole acidic region in Ca^{2+} binding, one notion might be that the E1077K mutation mimics the Ca^{2+}-bound (*i.e.* sensitized) state of the channel. On the other hand, the addition of a negative charge at T1078 could help to attract and hold the positive calcium ions or transduce the Ca^{2+} signal further downstream. This interpretation would support the suggestion that this region is important both for TRPA1 inactivation and also for Ca^{2+}-dependent potentiation. Site-directed mutagenesis studies have previously shown that neutralizations at two basic residues predicted to be located in the distal helices H4 and H5, flanking the acidic C-terminal domain, Lys^{1071} and Lys^{1092}, are capable of significantly reducing the responsiveness of TRPA1 to allyl isothiocyanate at negative membrane potentials but also cause defects in its voltage-dependent gating (18). Mutations at the cysteine or histidine residues located in this region had no effect on TRPA1 activation (3). Therefore, together with our results, it appears that specific charged residues within the entire region between helices H4 and H5 may comprise an important functional unit which, depending on Ca^{2+} binding, transmits a chemical signal from the N terminus to the gate. The recent 16 Å resolution structure of TRPA1 indicates that covalent modifications within the N termini might bridge adjacent monomers and induce conformational changes in the cytoplasmic domains of TRPA1 that lead to channel gating (36). By looking at this structure, it is tempting to speculate that the C-terminal helices forming a symmetrical structure parallel to the membrane plane might be stabilized by interactions between the positively charged region Lys^{988}–Arg^{1011} and the acidic cluster of the adjacent subunit. Upon Ca^{2+} binding, this interaction is disrupted, which might result in the opening of the channel.

The third key finding of this study provides essential evidence that the cluster of acidic residues in the TRPA1 cytosolic C terminus plays an important role in Ca^{2+}-dependent modulation and may represent a candidate region for the site of Ca^{2+} binding. This portion of the TRPA1 protein does not possess a "classical" Ca^{2+}-binding motif; thus our homology model cannot lend any direct structural support for identifying the Ca^{2+}-binding site. However, this model does fit the requirements for the ^{1074}IISETEDDDS^{1083} motif being a Ca^{2+}-binding loop; it provides a basis for additional structural insights into the possible receptor-Ca^{2+} contacts and in general is consistent with our experimental results. According to our simulations, the two residues Asp^{1080} and Asp^{1082} are predicted to be crucial for binding calcium, whereas the side chains of Ile^{1074} and Glu^{1077} are in contact with the calcium ion using their main chain carbonyl oxygen atoms (Fig. 5*B*). Indeed, we identified residues

Glu^{1073}, Glu^{1077}, Asp^{1080}, Asp^{1081}, and Asp^{1082}, the specific properties of which are not involved in Cin activation, but all appear to be most important for the modulation of the TRPA1 channel by Ca^{2+}, thus supporting the homology model as a plausible structure. To gain additional information toward a possible structural explanation of our data, we conducted measurements in which we explored the effects of the charge-neutralizing double mutations E1077Q/E1079Q, E1079Q/D1081N, and D1080N/1082N. All of the double mutants did not produce measurable currents in response to any of the stimuli tested, supporting the structural importance of the acidic motif.

We can be reasonably certain that in most cases, the changes in the magnitudes of the responses to cinnamaldehyde or depolarizing voltage are not due to changes in expression levels or plasma membrane targeting, because (*a*) simultaneous application of voltage and Ca^{2+} revealed considerable differences in the relative cross-sensitization capacity between the mutants, (*b*) several mutants were more specifically responding to voltage, *i.e.* their current-voltage relationships were qualitatively different from that in the wild-type channel, and, moreover, (*c*) we found that the strong consensus phosphorylation motifs containing serine 1076 and threonine 1078 (^{1071}KMEI-I**S**ETEDD^{1081} and ^{1073}EIISE**T**EDDDS^{1083}), both predicted to be targeted by casein-kinase CK2 with similar probabilities to TRPP2 (NetPhorest Posterior probability of 0.6386 and 0.6261 *versus* 0.6453 (43)), unlike TRPP2 (32), do not constitute a cytosolic sorting motif involved in the trafficking and surface expression of TRPA1. The findings that the nonphosphorylatable mutations S1076A and T1078A and the phosphorylation-mimicking mutation S1076D generated near to wild-type phenotypes indicates that the functional changes caused by other substitutions in this region are likely to be steric or local, rather than related to changes in the membrane insertion of the channels. In any case, we cannot exclude the possible involvement of the identified residues in the recently proposed, but yet to be determined, mechanism by which localized Ca^{2+} influx upon TRPA1 activation controls channel functionality through its acute translocation to the membrane (14).

REFERENCES

1. Story, G. M., Peier, A. M., Reeve, A. J., Eid, S. R., Mosbacher, J., Hricik, T. R., Earley, T. J., Hergarden, A. C., Andersson, D. A., Hwang, S. W., McIntyre, P., Jegla, T., Bevan, S., and Patapoutian, A. (2003) ANKTM1, a TRP-like channel expressed in nociceptive neurons, is activated by cold temperatures. *Cell* **112,** 819–829
2. Jordt, S. E., Bautista, D. M., Chuang, H. H., McKemy, D. D., Zygmunt, P. M., Högestätt, E. D., Meng, I. D., and Julius, D. (2004) Mustard oils and cannabinoids excite sensory nerve fibres through the TRP channel ANKTM1. *Nature* **427,** 260–265
3. Hu, H., Bandell, M., Petrus, M. J., Zhu, M. X., and Patapoutian, A. (2009) Zinc activates damage-sensing TRPA1 ion channels. *Nat. Chem. Biol.* **5,** 183–190
4. Bandell, M., Story, G. M., Hwang, S. W., Viswanath, V., Eid, S. R., Petrus, M. J., Earley, T. J., and Patapoutian, A. (2004) Noxious cold ion channel TRPA1 is activated by pungent compounds and bradykinin. *Neuron* **41,** 849–857
5. Bautista, D. M., Movahed, P., Hinman, A., Axelsson, H. E., Sterner, O., Högestätt, E. D., Julius, D., Jordt, S. E., and Zygmunt, P. M. (2005) Pungent products from garlic activate the sensory ion channel TRPA1. *Proc. Natl. Acad. Sci. U.S.A.* **102,** 12248–12252
6. Macpherson, L. J., Geierstanger, B. H., Viswanath, V., Bandell, M., Eid, S. R., Hwang, S., and Patapoutian, A. (2005) The pungency of garlic. Activation of TRPA1 and TRPV1 in response to allicin. *Curr. Biol.* **15,** 929–934
7. Corey, D. P., García-Añoveros, J., Holt, J. R., Kwan, K. Y., Lin, S. Y., Vollrath, M. A., Amalfitano, A., Cheung, E. L., Derfler, B. H., Duggan, A., Géléoc, G. S., Gray, P. A., Hoffman, M. P., Rehm, H. L., Tamasauskas, D., and Zhang, D. S. (2004) TRPA1 is a candidate for the mechanosensitive transduction channel of vertebrate hair cells. *Nature* **432,** 723–730
8. Nagata, K., Duggan, A., Kumar, G., and García-Añoveros, J. (2005) Nociceptor and hair cell transducer properties of TRPA1, a channel for pain and hearing. *J. Neurosci.* **25,** 4052–4061
9. Sawada, Y., Hosokawa, H., Hori, A., Matsumura, K., and Kobayashi, S. (2007) Cold sensitivity of recombinant TRPA1 channels. *Brain Res.* **1160,** 39–46
10. Karashima, Y., Talavera, K., Everaerts, W., Janssens, A., Kwan, K. Y., Vennekens, R., Nilius, B., and Voets, T. (2009) TRPA1 acts as a cold sensor *in vitro* and *in vivo*. *Proc. Natl. Acad. Sci. U.S.A.* **106,** 1273–1278
11. Nilius, B., Prenen, J., and Owsianik, G. (2011) Irritating channels. The case of TRPA1. *J. Physiol.* **589,** 1543–1549
12. Cavanaugh, E. J., Simkin, D., and Kim, D. (2008) Activation of transient receptor potential A1 channels by mustard oil, tetrahydrocannabinol and Ca^{2+} reveals different functional channel states. *Neuroscience* **154,** 1467–1476
13. Patil, M. J., Jeske, N. A., and Akopian, A. N. (2010) Transient receptor potential V1 regulates activation and modulation of transient receptor potential A1 by Ca^{2+}. *Neuroscience* **171,** 1109–1119
14. Schmidt, M., Dubin, A. E., Petrus, M. J., Earley, T. J., and Patapoutian, A. (2009) Nociceptive signals induce trafficking of TRPA1 to the plasma membrane. *Neuron* **64,** 498–509
15. Doerner, J. F., Gisselmann, G., Hatt, H., and Wetzel, C. H. (2007) Transient receptor potential channel A1 is directly gated by calcium ions. *J. Biol. Chem.* **282,** 13180–13189
16. Zurborg, S., Yurgionas, B., Jira, J. A., Caspani, O., and Heppenstall, P. A. (2007) Direct activation of the ion channel TRPA1 by Ca^{2+}. *Nat. Neurosci.* **10,** 277–279
17. Wang, Y. Y., Chang, R. B., Waters, H. N., McKemy, D. D., and Liman, E. R. (2008) The nociceptor ion channel TRPA1 is potentiated and inactivated by permeating calcium ions. *J. Biol. Chem.* **283,** 32691–32703
18. Samad, A., Sura, L., Benedikt, J., Ettrich, R., Minofar, B., Teisinger, J., and Vlachova, V. (2011) The C-terminal basic residues contribute to the chemical- and voltage-dependent activation of TRPA1. *Biochem. J.* **433,** 197–204
19. Xiao, Q., Prussia, A., Yu, K., Cui, Y. Y., and Hartzell, H. C. (2008) Regulation of bestrophin Cl channels by calcium. Role of the C terminus. *J. Gen. Physiol.* **132,** 681–692
20. Yuan, P., Leonetti, M. D., Pico, A. R., Hsiung, Y., and MacKinnon, R. (2010) Structure of the human BK channel Ca^{2+}-activation apparatus at 3.0 A resolution. *Science* **329,** 182–186
21. Susankova, K., Ettrich, R., Vyklicky, L., Teisinger, J., and Vlachova, V. (2007) Contribution of the putative inner-pore region to the gating of the transient receptor potential vanilloid subtype 1 channel (TRPV1). *J. Neurosci.* **27,** 7578–7585
22. Vlachová, V., Teisinger, J., Susánková, K., Lyfenko, A., Ettrich, R., and Vyklický, L. (2003) Functional role of C-terminal cytoplasmic tail of rat vanilloid receptor 1. *J. Neurosci.* **23,** 1340–1350
23. Dittert, I., Benedikt, J., Vyklický, L., Zimmermann, K., Reeh, P. W., and Vlachová, V. (2006) Improved superfusion technique for rapid cooling or heating of cultured cells under patch-clamp conditions. *J. Neurosci. Methods* **151,** 178–185
24. Thompson, J. D., Higgins, D. G., and Gibson, T. J. (1994) CLUSTAL W. Improving the sensitivity of progressive multiple sequence alignment through sequence weighting, position-specific gap penalties and weight matrix choice. *Nucleic Acids Res.* **22,** 4673–4680
25. Sali, A., Potterton, L., Yuan, F., van Vlijmen, H., and Karplus, M. (1995) Evaluation of comparative protein modeling by MODELLER. *Proteins* **23,** 318–326
26. Case, D. A., Darden, T. A., Cheatham, T. E., III, Simmerling, C. L., Wang,

J., Duke, R. E., Luo, R., Walker, R. C., Zhang, W., Merz, K. M., Roberts, B., Wang, B., Hayik, S., Roitberg, A., Seabra, G., Kolossvai, I., Wong, K. F., Paesani, F., Vanicek, J., Liu, J., Wu, X., Brozell, S. R., Steinbrecher, T., Gohlke, H., Cai, Q., Ye, X., Wang, J., Hsieh, M. J., Cui, G., Roe, D. R., Mathews, D. H., Seetin, M. G., Sagui, C., Babin, V., Luchko, T., Gusarov, S., Kovalenko, A., and Kollman, P. A. (2010) *AMBER 11*, University of California, San Francisco

27. Phillips, J. C., Braun, R., Wang, W., Gumbart, J., Tajkhorshid, E., Villa, E., Chipot, C., Skeel, R. D., Kalé, L., and Schulten, K. (2005) Scalable molecular dynamics with NAMD. *J. Comput. Chem.* **26,** 1781–1802
28. Harvey, M., Giupponi, G., and De Fabritiis, G. (2009) ACEMD: Accelerated molecular dynamics simulations in the microseconds timescale. *J. Chem. Theory Comp.* **5,** 1632–1639
29. Feenstra, K. A., Hess, B., and Berendsen, H. J. C. (1999) Improving efficiency of large time-scale molecular dynamics simulations of hydrogen-rich systems. *J. Comp. Chem.* **20,** 786–798
30. Humphrey, W., Dalke, A., and Schulten, K. (1996) VMD. Visual molecular dynamics. *J. Mol. Graph.* **14,** 33–38
31. Cordero-Morales, J. F., Gracheva, E. O., and Julius, D. (2011) Cytoplasmic ankyrin repeats of transient receptor potential A1 (TRPA1) dictate sensitivity to thermal and chemical stimuli. *Proc. Natl. Acad. Sci. U.S.A.* **108,** E1184–E1191
32. Köttgen, M., Benzing, T., Simmen, T., Tauber, R., Buchholz, B., Feliciangeli, S., Huber, T. B., Schermer, B., Kramer-Zucker, A., Höpker, K., Simmen, K. C., Tschucke, C. C., Sandford, R., Kim, E., Thomas, G., and Walz, G. (2005) Trafficking of TRPP2 by PACS proteins represents a novel mechanism of ion channel regulation. *EMBO J.* **24,** 705–716
33. Latorre, R., Morera, F. J., and Zaelzer, C. (2010) Allosteric interactions and the modular nature of the voltage- and Ca^{2+}-activated (BK) channel. *J. Physiol.* **588,** 3141–3148
34. Lightstone, F. C., Schwegler, E., Allesch, M., Gygi, F., and Galli, G. (2005) A first-principles molecular dynamics study of calcium in water. *Chemphyschem* **6,** 1745–1749
35. Javaherian, A. D., Yusifov, T., Pantazis, A., Franklin, S., Gandhi, C. S., and Olcese, R. (2011) Metal-driven operation of the human large-conductance voltage- and Ca^{2+}-dependent potassium channel (BK) gating ring apparatus. *J. Biol. Chem.* **286,** 20701–20709
36. Cvetkov, T. L., Huynh, K. W., Cohen, M. R., and Moiseenkova-Bell, V. Y. (2011) Molecular architecture and subunit organization of TRPA1 ion channel revealed by electron microscopy. *J. Biol. Chem.* **286,** 38168–38176
37. Kremeyer, B., Lopera, F., Cox, J. J., Momin, A., Rugiero, F., Marsh, S., Woods, C. G., Jones, N. G., Paterson, K. J., Fricker, F. R., Villegas, A., Acosta, N., Pineda-Trujillo, N. G., Ramírez, J. D., Zea, J., Burley, M. W., Bedoya, G., Bennett, D. L., Wood, J. N., and Ruiz-Linares, A. (2010) A gain-of-function mutation in TRPA1 causes familial episodic pain syndrome. *Neuron* **66,** 671–680
38. Salazar, M., Moldenhauer, H., and Baez-Nieto, D. (2011) Could an allosteric gating model explain the role of TRPA1 in cold hypersensitivity? *J. Neurosci.* **31,** 5554–5556
39. Smith-Maxwell, C. J., Ledwell, J. L., and Aldrich, R. W. (1998) Role of the S4 in cooperativity of voltage-dependent potassium channel activation. *J. Gen. Physiol.* **111,** 399–420
40. Brauchi, S., Orta, G., Mascayano, C., Salazar, M., Raddatz, N., Urbina, H., Rosenmann, E., Gonzalez-Nilo, F., and Latorre, R. (2007) Dissection of the components for PIP2 activation and thermosensation in TRP channels. *Proc. Natl. Acad. Sci. U.S.A.* **104,** 10246–10251
41. Boukalova, S., Marsakova, L., Teisinger, J., and Vlachova, V. (2010) Conserved residues within the putative S4-S5 region serve distinct functions among thermosensitive vanilloid transient receptor potential (TRPV) channels. *J. Biol. Chem.* **285,** 41455–41462
42. Voets, T., Owsianik, G., Janssens, A., Talavera, K., and Nilius, B. (2007) TRPM8 voltage sensor mutants reveal a mechanism for integrating thermal and chemical stimuli. *Nat. Chem. Biol.* **3,** 174–182
43. Miller, M. L., Jensen, L. J., Diella, F., Jørgensen, C., Tinti, M., Li, L., Hsiung, M., Parker, S. A., Bordeaux, J., Sicheritz-Ponten, T., Olhovsky, M., Pasculescu, A., Alexander, J., Knapp, S., Blom, N., Bork, P., Li, S., Cesareni, G., Pawson, T., Turk, B. E., Yaffe, M. B., Brunak, S., and Linding, R. (2008) Linear motif atlas for phosphorylation-dependent signaling. *Sci. Signal.* **1,** ra2